

Efficient and Accurate Description of Diels-Alder Reactions using Density Functional Theory

Daniele Loco,^{†,‡} Isabelle Chataigner,^{†,¶} Jean-Philip Piquemal,^{*,†} and Riccardo Spezia^{*,†}

[†]*Sorbonne Université, Laboratoire de Chimie Théorique, UMR 7616 CNRS, 4 Place Jussieu, 75005 Paris (France).*

[‡]*Qubit Pharmaceuticals, Incubateur Paris Biotech Santé, 24 rue du Faubourg Saint Jacques 75014 Paris (France).*

[¶]*Normandie Univ., UNIROUEN, CNRS, INSA Rouen, COBRA, 76000 Rouen (France).*

E-mail: jean-philip.piquemal@sorbonne-universite.fr; riccardo.spezia@sorbonne-universite.fr

Abstract

Modeling chemical reactions using Quantum Chemistry is a widely used predictive strategy capable to complement experiments in order to understand the intrinsic mechanisms guiding the chemicals towards the most favorable reaction products. However, to do so, it is mandatory to use reliable and computationally tractable theoretical methods. In this work, we focus on six Diels-Alder reactions of increasing complexity and perform an extensive benchmark of middle- to low-cost computational approaches to predict the characteristic reactions energy barriers. We found that Density Functional Theory, using the ω B97XD, LC- ω PBE, CAM-B3LYP, M11 and MN12SX functionals, with empirical dispersion corrections coupled to an affordable 6-31G basis set, provides quality results for this class of reactions, at a small computational effort.

Such efficient and reliable simulation protocol opens perspectives for hybrid QM/MM molecular dynamics simulations of Diels-Alder reactions including explicit solvation.

Introduction

The Diels-Alder reaction, first observed in 1928 by Otto Diels and Kurt Alder, has long been established as a key transformation in the toolbox of chemists. This two-bond-forming pericyclic combination of a 1,3-diene (4π component) with a dienophile (2π component) allows the formation of six-membered rings with well-defined regio- and stereo-chemistries and tolerates a large variety of functionalities. It is therefore not surprising that its applications in synthesis are numerous, going from the access to small, highly functionalized building blocks to the construction of complex natural products or polymers.^{1,2}

The possibility of describing these reactions via chemical simulations is thus of crucial importance. For example, it makes possible to understand (and predict) solvation effects or to model the role of pressure in tuning stereo-selectivity.³⁻⁶ At this end, computational chemists are often faced to deal with relatively large systems, either because the reactants are complex and extended, or because the solvent must be explicitly considered. One example of this last case, was reported recently by us showing that to understand pressure effects one needs to use molecular dynamics simulations within a mixed quantum mechanics - molecular mechanics (QM/MM) approach.⁶⁻⁸ Also, chemical dynamics simulations are often performed to elucidate the nature of mechanisms in organic reactions, for example to distinguish between synchronous or step-wise mechanisms,^{9,10} to elucidate post transition state dynamics,¹¹⁻¹⁴ or to understand kinetic isotopic effects,¹⁵ and this technique needs a large statistical sampling to have converged and robust results.

To allow the simulations of extended systems, two approaches are tempting: (i) using small basis sets in conjunction with electronic structure, both using Density Functional Theory (DFT) or Hartree-Fock (HF); (ii) using semi-empirical Hamiltonians (SEHs). In fact, the basis set size remarkably affects the computational cost of electronic structure calculations, while large basis are required, *e.g.*, in *ab initio* methods. To reach a sufficient accuracy, some DFT functionals might require very large basis sets.¹⁶ Given this constraint, MD simulations rapidly start to be unfeasible for real life applications, where a large phase

space needs to be sampled.

DFT was widely used to computationally study Diels-Alder reactions, and in a seminal work by Houk and co-workers it was pointed out that the popular B3LYP functional is not able to correctly describe single bond formation and double bond breaking.¹⁷ Since then, the developments of range-separated functionals and inclusion of dispersion made DFT more reliable and other functionals (like ω B97XD or M06-2X) are largely used in physical organic chemistry. Later, Grimme and co-workers pointed out how results of popular B3LYP functional on a set of organic reactions can be improved adding dispersion corrections.¹⁸ However, the search for reliable and/or computationally cheap basis sets is an important task in the field.¹⁹

SEHs were largely used in the past and replaced by modern theories when DFT calculations became available. However, in last years research in optimizing them was still active and they are still useful to address complex chemical reactions when a huge number of calculations are needed, like is the case when studying unimolecular dissociation in conjunction with mass spectrometry.^{20,21}

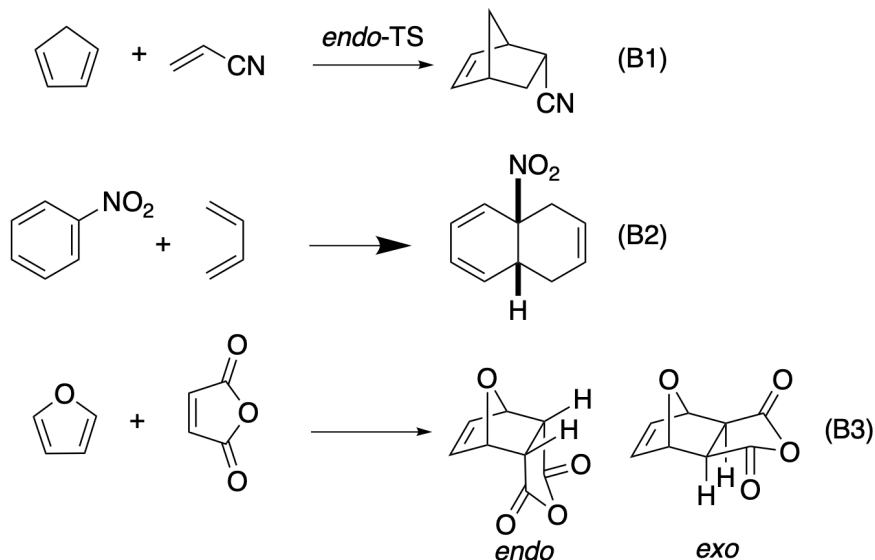
Of course these two options do not cover all the spectrum of possibilities, for example tight-binding DFT shows recently that it is able to deal with chemical reaction dynamics.^{22,23} Another possibility is also to train and/or use a machine learning algorithm for chemical reactions.²⁴ While some attempts to use this technique have been performed to predict activation energies,²⁵ it is at a preliminary stage and will need a huge data-set. Very recently, some reactive force-fields were developed with a first application also to a simple Diels-Alder reaction, but, at the present stage, this method needs a specific parametrization for each reaction.¹⁰ Surely, this approach will have interesting future applications in the field of organic reactions, but it needs, at the present stage, further development and more grounded common and standard utilities.

Nowadays organic chemistry can maximize the efficiency of well-known and studied approaches like DFT, HF or SEHs. At this end, we investigated how accurate is the description

of Diels-Alder reactions using such relatively fast methods. We have first studied a set of benchmark calculations on well-established Diels-Alder reactions and then applied to specific (4+2) cycloadditions where the dienophiles are strained cyclic allene for which both experimental and very recent calculations are reported.²⁶⁻²⁹

Prototypical Diels-Alder cycloadditions (see reactions B1-B3 in Scheme 1) were selected for this benchmark. These small systems were chosen in order to be able to perform highly-correlated reference calculations (here at CCSD(T) level of theory). We thus chose three reactions involving cyclic or acyclic dienes, aromatic or non- aromatic substrates, and dienophiles bearing different types of classical electron-withdrawing groups (cyano, nitro and ester/anhydride). This led us to select B1 involving cyclopentadiene and acrylonitrile, a classical reaction that we had recently studied computationally under high pressure.⁶ In B2 cycloaddition, butadiene reacts with nitrobenzene as aromatic dienophile, a reaction linked to our interest in (4+2) Diels-Alder cycloaddition with electron-poor aromatic compounds.³⁰⁻³⁵ Note that in this case the cyclo-adduct will not differ by *endo* or *exo* approach, while the TS will. Here we consider the TS approach corresponding to the conformation which is lower in energy (the aromatic ring and the diene on the same side). Finally, B3 reaction involves the classical Diels-Alder between furan and maleic anhydride to form norcantharidin, whose *endo/exo* diastereoselectivity under kinetic/thermodynamic control has been debated over years.³⁶⁻³⁸

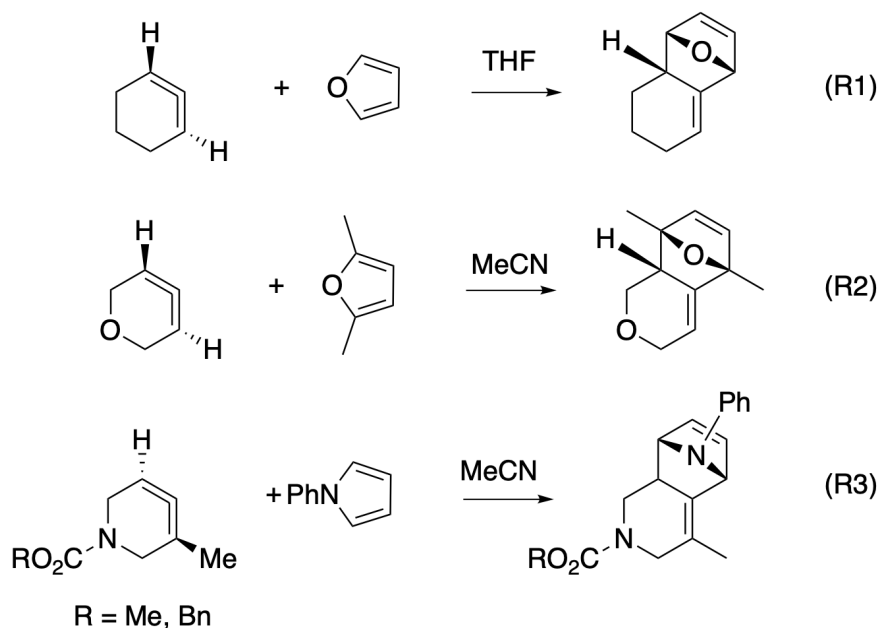
Recently, Houk and co-workers have studied computationally a class of Diels-Alder reactions in which the dienophile has a cyclic allene structure.²⁶ They are particularly interesting because it is possible to synthesize several stereochemically-reach products in this way. This is possible thanks to the high *endo:exo* ratio as reported by many experiments.^{27-29,39,40} Quantum chemistry calculations provide a key tool to understand and predict such *endo:exo* ratio. Our theoretical results can be compared with such experimental data in addition to the aforementioned calculations which use DFT with an extended basis set which would be computationally not affordable in further and likely QM/MM molecular dynamics simula-



Scheme 1: Reactions under consideration in benchmark calculations.

tions. We have thus selected three reactions among those studied by Houk and co-workers and reported in Scheme 2.

The first reaction (R1) is one of the simplest possible: furan reacts with cyclohexa-1,2-diene yielding 80% of products with an *endo:exo* ratio of 11:1.²⁷ This selectivity is notable because it arises from “a new type of secondary orbital interaction that results from the near perpendicular approach of the diene to the dienophile and the twisted nature of the strained allene”.²⁶ We have then chosen two other reactions, R2 where the reactants were slightly modified, resulting in similar *endo:exo* ratio (9.2:1),²⁸ and R3 where experimentally only the *endo* adduct was observed.²⁹ The aforementioned calculations reported recently, done with the ω B97XD and a relatively large basis set (6-311+G(d,p)) in implicit solvent, found a relatively small *endo:exo* ratio (3.3:1)²⁶ which is even smaller than what obtained for R1 and R2 reactions. Note that calculations were done with R=Me (methyl group), while experiments were done with R=Bn (benzyl group). The use of a smaller basis set would allow to easily check if the use of the benzyl group as in experiment in conjunction with the best performing functionals can bridge this gap.



Scheme 2: Diels-Alder reactions with a strained cyclic allene dienophile considered in this study. R1 is done in THF, while R2 and R3 in acetonitrile (MeCN).

Computational details

Reactions under consideration

The reactions studied are reported in Schemes 1 and 2, where the nomenclature used here and hereafter for the different reactions is also depicted. All calculations described in the following were done with Gaussian 16⁴¹ and Mopac16⁴² (for semi-empirical Hamiltonians) software packages.

Reference calculations

Reference energies have been obtained applying the following recipe: pre-complex (PreC) and transition state (TS) structures are optimized using the best level available, given the size of the system; the CCSD(T) energy at the Complete Basis Set (CBS) limit is then obtained performing a two-points extrapolation procedure on the correlation energy only,⁴³ using those fixed structures. The largest affordable basis sets for the two points extrapolation have been used, typically the cc-pVDZ and cc-pVTZ Dunning's basis sets. The basis set superposition

error (BSSE) counterpoise correction is applied in the CCSD(T) total energy calculations, from which a BSSE-corrected correlation energy is extracted. Just for Reaction B1 the calculations were affordable also using the aug-cc-pV(D,T)Z basis sets, and the resulting extrapolated CBS energy has been reported in the SI (see Table S2).

The final CCSD(T)/CBS reference energy is obtained adding such BSSE-corrected, extrapolated correlation energy to a reference state energy computed at the HF/aug-cc-pV5Z level,⁴⁴ so to reasonably account for any source of error coming from incomplete basis sets, including the BSSE also for the non-correlation part of the total electronic energy. This is shown to be a reasonable assumption for Reaction B1, where HF energies at aug-cc-pVQZ, aug-cc-pV5Z and aug-cc-pV6Z are compared, showing a quite low impact of basis set related errors already at the quadruple- ζ (see SI, Section S1) , and a quite small variation passing from quintuple- ζ to 6- ζ (see SI, Table S1). In Section S1 of the SI more details are reported on this topic and on the reference energies calculations in general.

DFT calculations

We have used different functionals, listed in Table 1 where we classified them by type and where we specified if dispersion is also added and with which method. For dispersion, we used the D3BJ correction⁴⁵ when available for the given functional otherwise we used D2⁴⁶ or D3,⁴⁷ as specified in the same Table 1.

We used different basis sets, and namely: STO-3G, 3-21G, 6-31G, 6-31G(d,p) and 6-311++G(d,p). BSSE was calculated using the counterpoise method of Boys and Bernardi.⁸⁷

In the case of reactions involving strained cyclic allene dienophiles, we performed also calculations in implicit solvent using the SMD solvation model⁸⁸ as in the recent work by Houk and co-workers.²⁶

Table 1: Functional used in the benchmarking. We classified them in the Type column using the following abbreviations: local spind density approximation (LSDA), generalized gradient approximation (GGA), hybrid GGA (HGGA), meta-GGA (mGGA), hybrid-meta-GGA (HmGGA), range-separated hybrid (RS), non-separable gradient approximation (NGA), double hybrid (DH). When dispersion correction is added this is reported in the specific column, in parenthesis if the functional is used both with and without dispersion.

Functional	Dispersion correction	Type	References
SVWN	–	LSDA	48–50
BLYP	(D3BJ)	GGA	51–53
PBE	(D3BJ)	GGA	54
HCTH/407		GGA	55
B97	D2, D3	GGA	56,57
G96LYP		GGA	52,53,58
BP86	D3BJ	GGA	51,59
SOGGA11		GGA	60
B3LYP	(D3BJ)	HGGA	52,53,61
PBE0	(D3BJ)	HGGA	62
B3PW91		HGGA	61,63
B1B95		HGGA	64
mPW1PW91		HGGA	65
mPW1PBE		HGGA	54,65
mPW3PBE		HGGA	54,65
B3PW91	D3BJ	HGGA	61,63
APFD		HGGA	66
SOGGA11X		HGGA	67
TPSS	D3BJ	mGGA	68
VSXC		mGGA	69
τ HCTH		mGGA	70
M06-L		mGGA	71
M06		HmGGA	72
M06HF		HmGGA	73
τ HCTH _{hyb}		HmGGA	70
BMK	D3BJ	HmGGA	74
CAM-B3LYP	(D3BJ)	RS-HGGA	75
ω B97XD	D3	RS-HGGA	76
ω B97		RS-HGGA	77
HSEH1PBE		RS-HGGA	78
OHSE1PBE		RS-HGGA	78
OHSE2PBE		RS-HGGA	78
HISSbPBE		RS-HGGA	79
LC- ω PBE	(D3BJ)	RS-HGGA	80
N12SX		RS-HGGA	81
M11		RS-HmGGA	82
MN12SX		RS-HmGGA	81
N12		NGA	83
M11-L		mNGA	84
MN12-L		mNGA	85
B2PLYP	(D3BJ)	DH-GGA	86

Wave-function and Semi-empirical Hamiltonians

We have also considered Hartree-Fock (HF) and MP2 methods to compare with DFT and reference CCSD(T) calculations, varying also in those cases the basis set size, in the benchmarking calculations. Furthermore, we have tested some popular semi-empirical Hamiltonians (SEHs) which are computationally much faster than DFT and are thus tempting as method, in particular in molecular dynamics simulations. At this end we have considered the following methods: AM1,⁸⁹ AM1-D, RM1,⁹⁰ RM1-D, PM3,⁹¹ PM6,⁹² PM6-D, PM6-D3, PM6-D3H4⁹³ and PM7,⁹⁴ where D and D3 stand for the D⁹⁵ and D3⁴⁷ methods by Grimme, respectively.

Results and Discussion

Basis Set Effect

We first consider in detail the role of the basis set superposition error (BSSE) in particular concerning energy barriers. This will be important to understand also the role of the intrinsic error of a finite basis set. DFT calculations are here compared with CCSD(T)/CBS results which are taken as reference for both method and basis set.

First we consider the activation energy of reactions B1 and B2. The activation energy

$$E^{\text{a}} = E_{\text{TS}} - E_{\text{PreC}} \quad (1)$$

is calculated considering as the starting point the non-covalent complex formed by the reactants (PreC). Note that the PreC is obtained once from an intrinsic reaction coordinate (IRC) calculation from the TS structure corresponding to the reactant state and the resulting structure is then directly optimized each time with the different methods.

For Reaction B1, which is the simplest system treated in this work, additional high-level electronic structure calculations are performed, to estimate the reliability of the reference

chosen. We notice that, as reported in Table S2 of the Supporting Information (SI), the CCSD(T) calculations with the larger basis sets used for the CBS extrapolation are almost identical to those which use the slightly smaller basis sets. We then use this last one extrapolation for the other reactions with good confidence.

It is relevant to observe here that the MP2/CBS (see Section S1 of SI for details) barrier provided in the SI is roughly half of the CCSD(T)/CBS one. Since the latter method is widely considered as a golden standard, the reason of such a huge mismatch can be ascribed to an erroneous prediction of MP2, which can be rooted in i) the more approximated treatment of correlation energy, particularly evident ii) in its known deficiency of describing accurately non-covalent interactions.

We present now how BSSE behaves for some functionals considered: we have chosen some between those who perform the best as discussed in the following subsections. Also other DFT functionals perform as well as the ones reported hereafter, and the exhaustive list of computed energy barriers including all tested functionals is reported in the SI (see Tables S5 and S6).

In Figure 1 the activation energy differences ($|\Delta E|^a$) computed with the selected functionals (M06-2X, MN12SX, B2PLYP and LC ω -PBE) with respect to the reference CCSD(T)/CBS values, are shown for Reactions B1 and B2. The effect of correcting for the BSSE or avoiding such a costly correction is analyzed. The non-BSSE corrected barriers (full symbols) all converge towards the reference values at the Pople 6-31G basis level, while they are very far from it for the smaller STO-3G and 3-21G basis, strongly underestimating the reaction barrier. This is due to the, by definition, always negative BSSE value, which stabilizes more the TS, for which BSSE values are larger (see Figure 1, BOTTOM panel) than the PreCs, for which the BSSE is smaller (same panel in Figure 1). For comparison, we also reported the BSSE corrected barrier differences (empty symbols), which are, as expected, always higher than the corresponding non-BSSE corrected ones. For the larger 6-311++G(d,p) basis, the difference between non-BSSE corrected and BSSE corrected barriers is obviously much smaller, so that

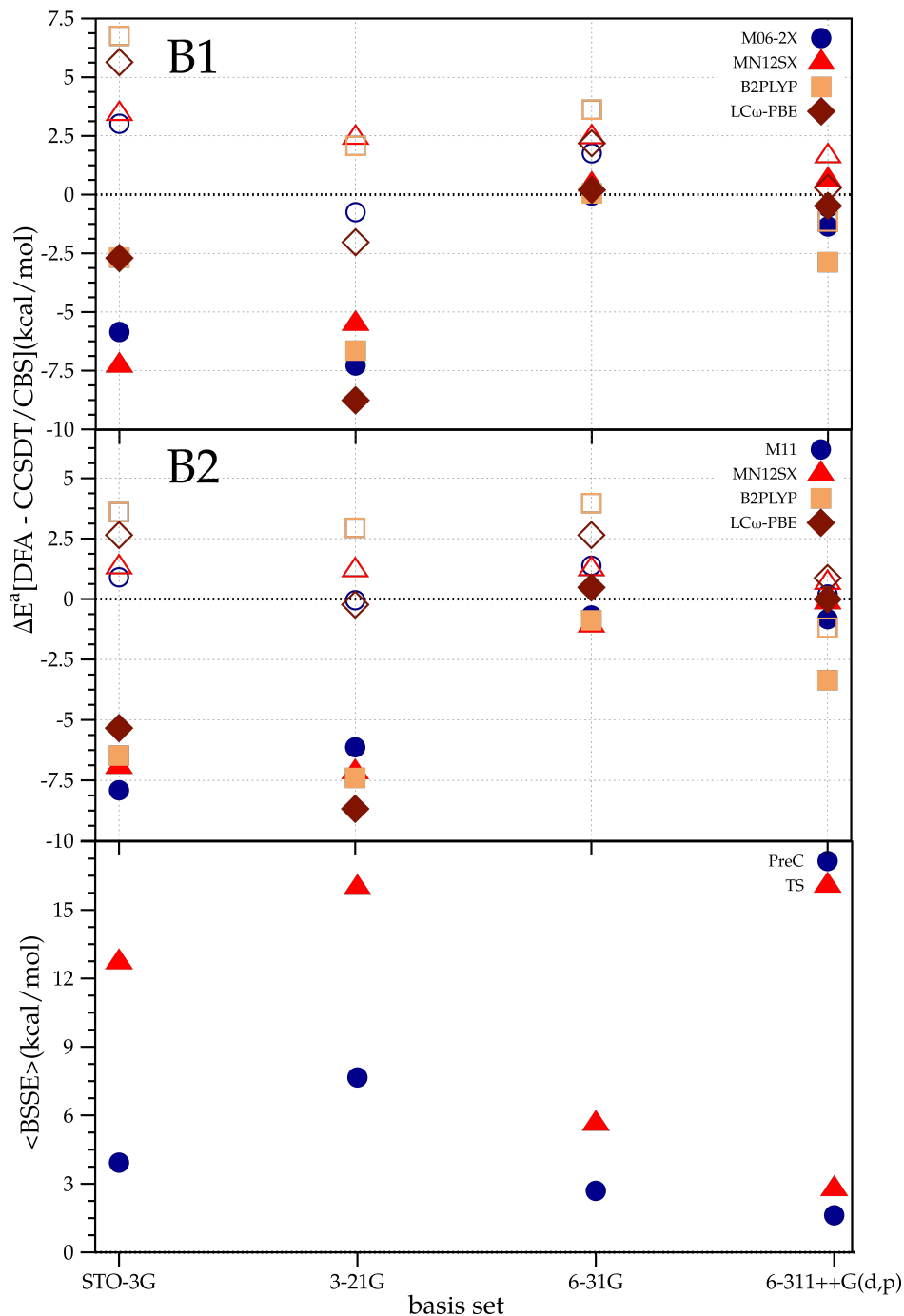


Figure 1: Gas-phase activation energy's basis set dependence for reactions B1 (TOP) and B2 (MIDDLE); we report the difference between reference CCSD(T)/CBS and the best DFT results (Density Functional Approximations, DFAs, as reported on the y-axis of the graphs). Non-BSSE corrected values (filled symbol) are compared with the BSSE corrected ones (empty symbol). Empirical dispersion (Grimme's D3BJ as implemented in the Gaussian suite⁴⁵) has been added to the non-Minnesota functionals; BOTTOM) average BSSE absolute values, averaging over the different functionals' computed energies, for both pre-complexes (PreC) and TSs

either one or the other, depending on the functional, reach a satisfactory agreement with the reference, in most of the cases between ± 2.5 kcal/mol.

In Figure 1 (BOTTOM panel) we report the BSSE value obtained averaging out the BSSE of each functional for each basis set. TSs show a much larger BSSE than PreCs, due to the generally larger inter-fragment distances which characterize the latter. As expected, the BSSE decreases from smaller to larger basis sets, with the maximum value for the 3-21G basis, with an average BSSE of 16 and 8 kcal/mol for TSs and PreCs, respectively. The minimal STO-3G basis shows a quite smaller BSSE values, 13 for TSs and 4 kcal/mol for PreCs, compared to the smallest Pople's basis set tested, the 3-21G. This fact can be interpreted as a smaller overlap between basis from different fragments when using STO-3G.

We also remark here that the BSSE correction applied to 3-21G calculations (TOP and MIDDLE panels in Figure 1, empty symbols) brings the results of the selected functionals close, or at least much closer than the non-BSSE corrected ones, to the reference. On the opposite the STO-3G results show in almost all cases a quite bad agreement with the reference. All in all, the reduced BSSE (see BOTTOM panel in Figure 1) improves the intrinsic behavior of DFT, so that BSSE corrected and non-BSSE corrected values are generally improved in the 6-31G and the 6-311++G(d,p) basis sets over the STO-3G and the 3-21G. In particular for the 6-31G basis the reduced BSSE (still larger than those of 6-311++G(d,p)) compensates for the intrinsic error of the DFT functionals, surprisingly giving a very good agreement between the reference (CBS) and the non-BSSE corrected barriers.

It is worth spending few words to quantify the time needed to perform these calculations.

Table 2: computational time ratios for Reaction B1; we reported the slow-down factor to complete a gas-phase SCF procedure when passing from the 6-31G basis set without BSSE correction (6-31G-NoCorr) to the largest tested 6-311++G(d,p) basis including or not BSSE counterpoise corrections (6-311++G(d,p)-Corr/NoCorr). The slow-down factors are computed for calculations on both TS and pre-complex (PreC). The time factor is computed as $\frac{t(\mathcal{B})}{t(6-31G-NoCorr)}$, with \mathcal{B} one of the basis set reported in the left-most column of the table, including or not BSSE corrections

	TS		PreC	
	MN12SX	B2PLYP/D3BJ	MN12SX	B2PLYP/D3BJ
6-31G-NoCorr	1.0	1.0	1.0	1.0
6-31G-Corr	3.0	3.3	2.4	3.3
6-311++G(d,p)-NoCorr	5.4	14.4	4.8	10.9
6-311++G(d,p)-Corr	16.5	32.8	14.2	48.6

In Table 2 we report the slow-down time factor for an SCF energy evaluation in gas-phase using the 6-311++G(d,p) basis, with and without BSSE counterpoise correction, with respect to the 6-31G one. The calculations are performed for both TS and PreC structures of Reaction B1, and we also include 6-31G calculations with BSSE correction. We chose to use two of the best working functionals, as discussed later, the MN12SX and the B2PLYP including empirical dispersion, but the conclusions we draw, reasonably, are not significantly affected by this choice. For both functionals, a slow-down factor between 3 and 15 is found for the 6-31G basis with BSSE and 6-311++G(d,p) basis without BSSE correction. For the 6-311++G(d,p) basis with BSSE correction the slowing factor is much higher in average, being ~ 48 in the worst case, for the PreC treated with the B2PLYP/D3BJ method.

If one is interested in simulating the dynamics of the system, even an apparently small factor, as a 2 or 3 slower calculation, can determine a drastic reduction in the number of dynamics steps that one can afford, reducing the portion of the phase space of the system that one can explore and consequently the reliability of calculated quantities.

Activation energies on benchmark reactions

In light of this preliminary analysis on the BSSE effect on the reaction barriers computed for two of the Diels-Alder reactions in Scheme 1, we extended the set of tested functionals to find good cost-effective methods to predict a reliable energy barrier. First we have considered the gas-phase barrier for reactions B1 and B2 comparing the DFT results with reference CCSD(T)/CBS calculations. Note that, since CCSD(T)/CBS calculations provide only electronic energies, here we compare this quantity without considering any contribution from molecular vibrations (typically to free energies): they will be added when studying the reactions with strained cyclic allene dienophiles in the last subsection. As shown in the previous subsection, STO-3G basis set provides very poor results and thus we did not include it in further comparisons.

The full set of results obtained from 3-21G, 6-31G, 6-31G(d,p) and 6-311++G(d,p) basis sets with different functionals for Reactions B1 and B2 are reported in Tables S3 and S4 in the SI where we also compare with CCSD(T)/CBS values. Note that for reaction B1 we report, for many functionals excluding the Minnesota class, values with and without dispersion correction. In general, dispersion decreases the barriers: when they are overestimated without dispersion they tend to become closer to the reference value, but the improvement is not generalized.

When dealing with reaction B2, the structures of the PreC are often totally wrong if dispersion is not included. In Figure 2 we show as an example the PreC obtained at B3LYP/6-31G level of theory with and without dispersion correction. We should remind that here we define a PreC as a structure which is formed when the reactants approach to each other and technically obtained by following the intrinsic reaction coordinate (IRC) backward to reactants from the TS down to the first minimum. In other terms, the PreC by definition should have a structure where the reactants are close together “ready” to form the TS (corresponding substrates in almost parallel plans in our case dealing with a Diels-Alder cycloaddition), which in the present case is what obtained when dispersion correction is added. On the other

hand, when the dispersion is not included, the geometry is totally unrealistic, with substrates lying in perpendicular planes in the present case. The same behavior is observed with almost all the functionals and basis sets, but the Minnesota families of functionals, which are able to catch, in our application, the good behavior without adding empirical dispersion. The qualitatively good description of dispersion of the Minnesota functionals can be ascribed to their specific functional form, and thanks to the detailed and extended fitting procedure applied to evaluate the parameters which are involved in their definition.^{96,97} With this consideration, and verifying that PreC and TS structures do not undergo significant distortion, we did not add dispersion correction when using Minnesota functionals.

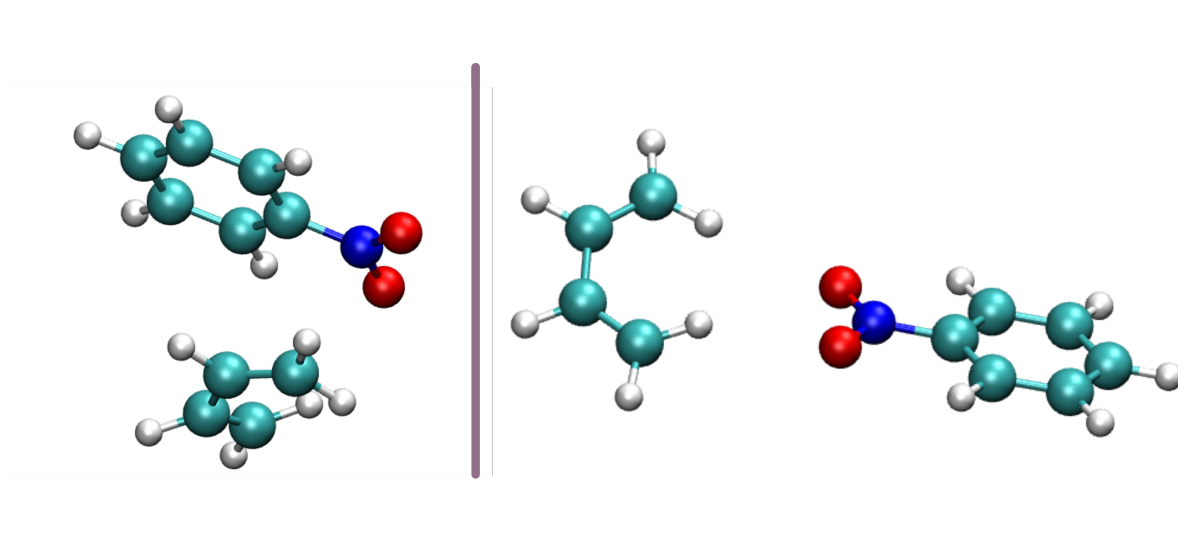


Figure 2: Pre-complex structures for Reaction 2 using B3LYP-D3BJ/6-31G (left) and B3LYP/6-31G (right).

Results with the small 3-21G basis set are largely off, the best being ω B97XD for Reaction B1 and CAM-B3LYP/GD3BJ for Reaction B2, which are underestimated by 2.16 and 5.31 kcal/mol, respectively. When moving to 6-31G basis set the results are largely better: many functionals provide energy barriers which are different by less than 1 kcal/mol with respect to CCSD(T)/CBS reference. In particular, range-separated functionals (ω B97XD, M11, LC- ω PBE and MN12SX) are able to provide barriers which are very close to the reference value. The double hybrid B2PLYP/D3BJ functional also provides excellent results

with such relatively small basis set. Note that also other Minnesota functionals are able to provide good results, in particular for Reaction B2. Notably, when we just add polarization functions, the situation is not improved, and the same classes of functionals provide the best results. The 6-31G(d,p) basis set does not improve the quality of the results while it is computationally more expensive, even if slightly. Note that this is particularly important for molecular dynamics simulations when many energy and gradient calculations are needed and thus this can result in a huge difference from a computational point of view.

The same picture arises with a larger basis set, 6-311++G(d,p), for which again range-separated functionals (in particular LC- ω PBE, M11 and MN12SX) provide the barriers in better agreement with the reference values.

We now move to results for reaction B3, for which we have calculated the transition states for both *endo* and *exo* forms, and thus we can compare those two values and the difference between them. Values obtained with different basis sets (here we did not consider the smallest 3-21G basis which, as we have shown, provides too poor results) and functionals are reported in Table S8 of the SI and compared with CCSD(T)/CBS results. Here again, 6-31G and 6-31G(d,p) results are very similar and there is not a clear improvement adding polarization functions. Again long-range corrected and screen-exchanged functionals provide very good results. Notably, the global hybrid GGA SOGGA11X functional provides very good results with both 6-31G and 6-31G(d,p) basis sets. When moving to the 6-311++G(d,p) large basis set, the range-separated functionals (and in particular CAM-B3LYP/D3BJ, ω B97XD, MN12L and MN12SX) work best. Concerning the *endo:exo* energy difference, the reference CCSD(T)/CBS reports a very small value (0.48 kcal/mol) which could be very difficult to reproduce accurately with an approximated electronic structure method. Notably, almost all calculations reproduce the correct sign, with very few exceptions (τ HCTC/6-31G(d,p), τ HCTC/6-311++G(d,p) and M06HF/6-31G(d,p)) in which the difference is very small (0.15 kcal/mol or less).

Before discussing the energetic of two analogous Diels-Alder reactions in solution, we

should pause and consider the global behavior of all these functionals at a given basis set. Since we have a relatively large number of functionals, we can see how they behave on average and if the best functionals have a considerable deviation from such average. We report in Table 3 the mean signed and unsigned errors (MSE and MUE, respectively) together with the root mean square deviation (RMSD) as a function of the basis set for the different reactions, mixing all together (for reaction B3 we consider only one barrier to have only independent values). Notably, from 6-31G to 6-311++G(d,p) the MUE does not change dramatically (about 1 kcal/mol) and the RMSD is almost constant, thus strengthening the picture we have discussed previously. In fact, we can notice (again) that the 3-21G basis set systematically largely underestimates the barrier while 6-31G provides results close to (if not better than) 6-31G(d,p), and not significantly worse than 6-311++G(d,p), but with a much reduced computational effort.

Let’s now consider five functionals (all being range separated) which show a good behavior in the three benchmark reactions, namely: CAM-B3LYP/D3BJ, LC- ω PBE/D3BJ, ω B97XD, M11 and MN12SX.

6-31G basis set performances

As shown and discussed in the previous subsection, 6-31G basis set seems to be a good compromise. We now discuss in more details the performances of the different functionals with this basis set in order to provide a limited set of functionals which will be more likely to be used in real applications.

In Figure 3 we report the absolute error obtained by the different functionals for the barrier of reaction B1 with respect to CCSD(T)/CBS results. Notably many functionals provide an error less than 1 kcal/mol with respect to the reference, and notably the double hybrid B2PLYP/D3BJ and the range separated ω B97XD, M11, M11L, LC- ω PBE/D3BJ, MN12SX, MN12L while CAM-B3LYP/D3BJ has a slightly bigger error (2 kcal/mol).

As discussed previously, for reaction B2 many functionals (actually all but Minnesota

Table 3: Mean signed and unsigned error (MSE and MUE, respectively) and root means square deviation (RMSD) for different basis sets and benchmark reactions (differences are with respect to CCSD(T)/CBS calculations). Values are in kcal/mol.

Reaction	Basis set	MSE	MUE	RMSD
B1	3-21G	-8.04	8.04	3.30
	6-31G	-0.70	2.54	3.19
	6-31G(d,p)	-2.25	3.16	3.27
	6-311++G(d,p)	-1.20	2.88	3.45
B2	3-21G	-11.36	11.36	4.18
	6-31G	-4.21	4.56	3.86
	6-31G(d,p)	-5.02	5.17	3.90
	6-311++G(d,p)	-3.99	4.46	3.90
B3-Endo	3-21G	-15.69	15.69	4.01
	6-31G	-4.88	5.09	3.25
	6-31G(d,p)	-5.21	5.36	3.25
	6-311++G(d,p)	-3.54	4.01	3.61
B3-Exo	3-21G	-15.36	15.36	3.81
	6-31G	-4.33	4.57	3.12
	6-31G(d,p)	-5.37	5.47	3.17
	6-311++G(d,p)	-3.56	3.95	3.51
B3- Δ	3-21G	-0.32	0.37	0.31
	6-31G	-0.54	0.54	0.21
	6-31G(d,p)	0.16	0.21	0.21
	6-311++G(d,p)	0.02	0.17	0.21
B1+B2+B3-Endo	3-21G	-10.90	10.90	0.49
	6-31G	-2.68	3.72	0.39
	6-31G(d,p)	-3.74	4.26	0.37
	6-311++G(d,p)	-2.54	3.58	0.39

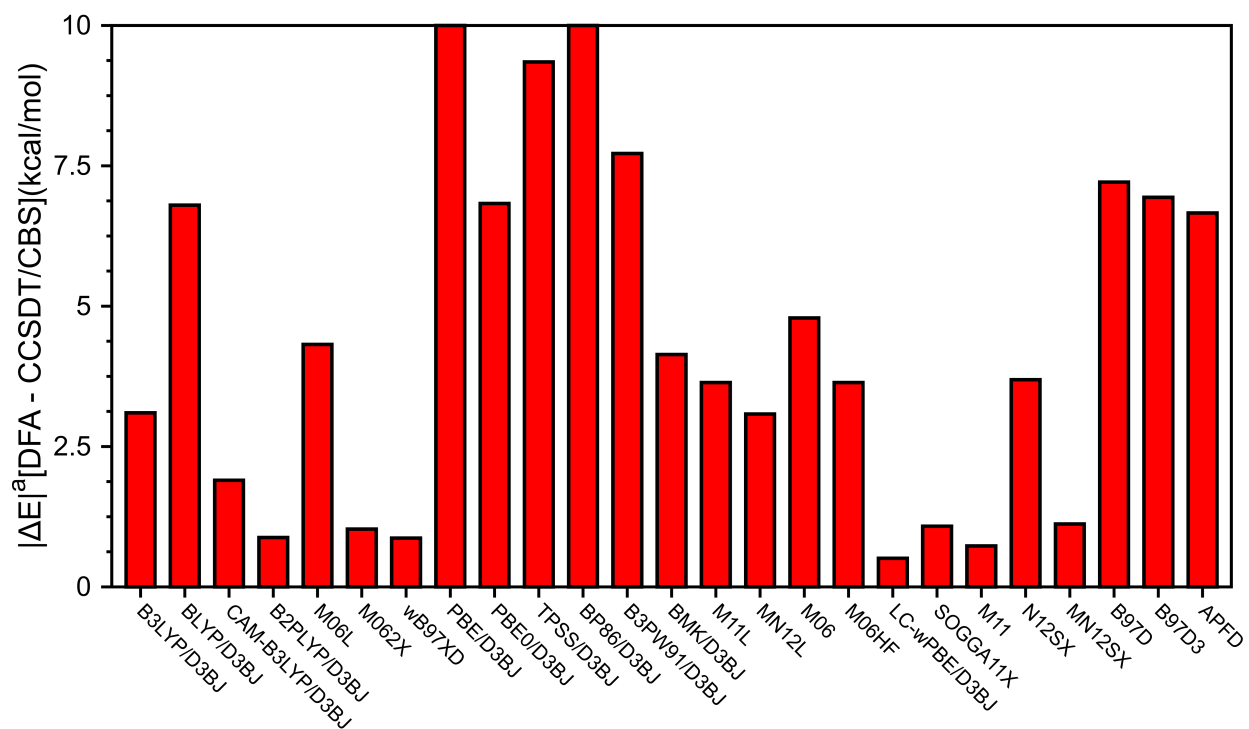


Figure 4: Absolute activation energy differences ($|\Delta E|^a$) between tested functionals (Density Functional Approximations, DFA on the y-axis) and the reference CCSD(T)/CBS, reported in kcal/mol, for 6-31G calculations for Reaction B2.

(~ 0.5 kcal/mol in the reference). On the other hand, few functionals are able to provide the *endo* energy barrier close to the reference value. Notably, τ HCTH barrier is very close to the reference, but this method provides, wrongly, a lower *exo* barrier. Other well behaving functionals are SOGGA11X, M06L, CAM-B3LYP/D3BJ and ω B97XD. Still in acceptable agreement with the reference, but slightly worse, are results obtained by the Minnesota MN12SX and the N12SX functionals, which give very similar results as the B2PLYP/D3BJ. Overall the results on the B3 reaction show less functionals in very good (close to 1.0-0.5 kcal/mol) agreement with the reference compared to the B1 and B2 cases, if we consider the absolute reaction barrier. However, concerning the difference between *endo* and *exo* barriers the general agreement is more satisfactory, as discussed in the previous section.

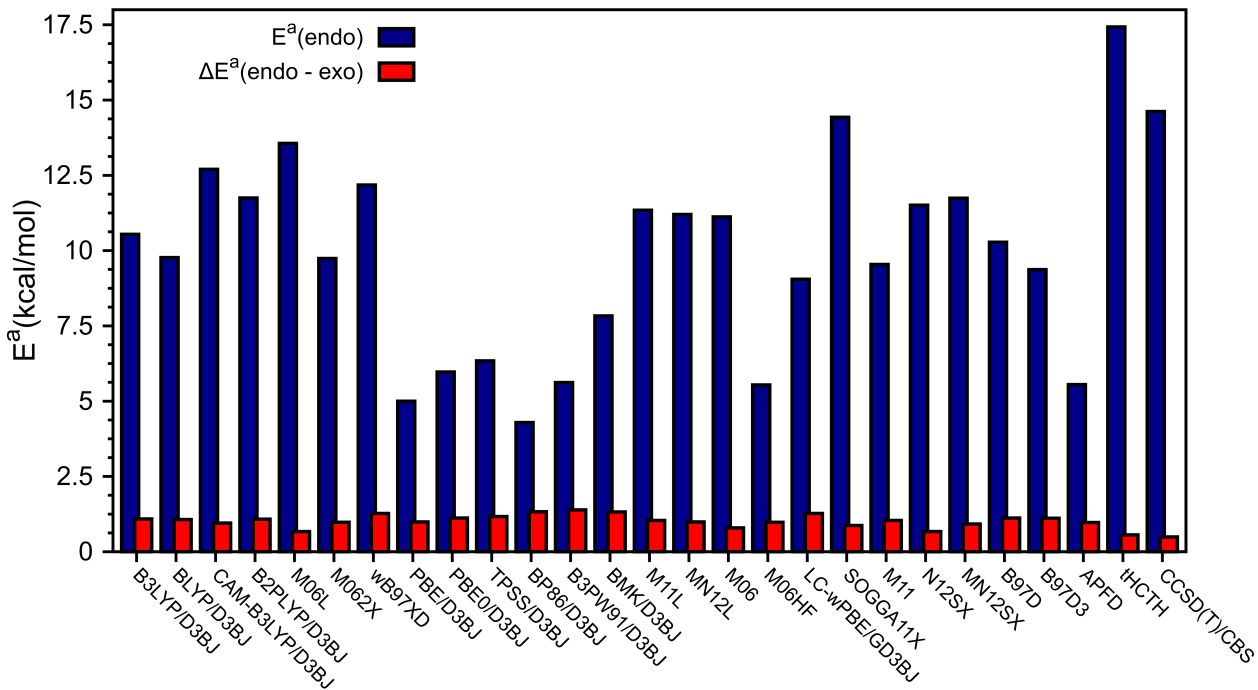


Figure 5: Absolute activation energies (E^a in blue) and differences between endo and exo activation energies ($|\Delta E|^a$ in red) for the B3 reaction, are reported in kcal/mol and computed with the many functionals reported on the x-axis always using the 6-31G basis set; the reference CCSD(T)/CBS corresponding values are also reported for comparison.

Semiempirical methods

In principle, Hartree-Fock (HF) and Semi-Empirical Hamiltonians (SEH) methods can provide an efficient way to evaluate reaction energetics, thanks to the much more favorable scaling with the size of the system if compared to MP2. We thus tested a number of SEHs and also HF with small basis sets. The full set of results are reported in Table S10 of SI, where we also report MP2 values with relatively small basis sets and reference calculations for the three benchmark reactions. In Figure 6 we show the results for SEHs and HF/6-31G calculations.

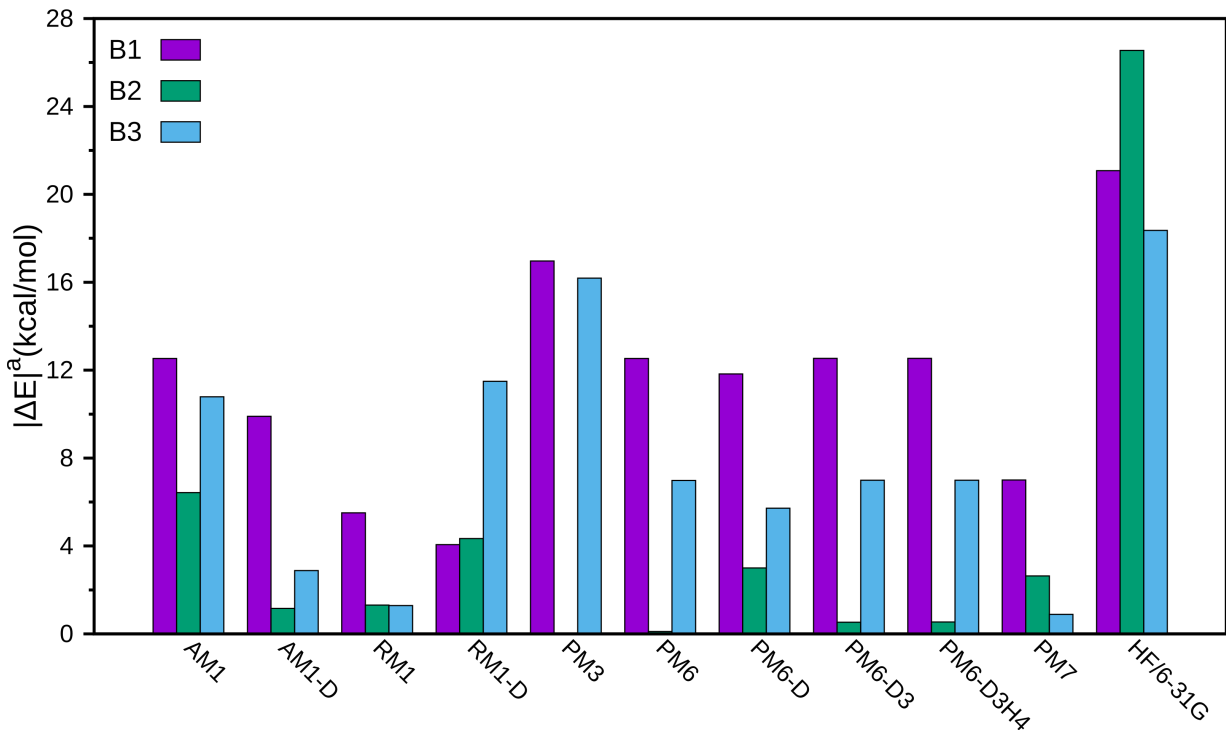


Figure 6: $|\Delta E|^a$ computed between the SEHs and HF/6-31G reaction barriers and the corresponding reference CCSD(T)/CBS reference value computed in this work.

As one can clearly notice from these results, the different methods show a poor agreement with respect to reference CCSD(T)/CBS calculations. For Reaction B2, we found that few SEHs, as the AM1-D, RM1, PM6-D3 and PM6-D3H4, reproduce quite well the reference, which is not the case for Reaction B1 nor B3, being probably due to fortuitous error corrections. Globally, a slight preference for RM1 or PM7 could be drawn, but the deviation

from the reference is too large to be used with confidence. Thus, we do not consider in the following neither HF nor SEH methods. Note that, HF in general shows probably the worst results between all the methods tested in this work.

Application to Strained Cyclic Allene Dienophiles

Given the results on benchmark reactions, we finally found that range separated functionals (CAM-B3LYP, LC- ω PBE, ω B97XD, M11 and MN12SX) show the best performances with 6-31G basis set, having computing time which are similar to standard functionals. Also the double-hybrid functional B2PLYP provides very good results, but it is much more computationally demanding, in particular when frequency calculations are needed and thus it will not be considered here. We have thus consider these range separated functionals plus the recently proposed SOGGA11X functional, which provides good performances with 6-31G basis set, to study some selected Diels-Alder reactions with a strained cyclic allene dienophile (see Scheme 2).

These reactions were recently studied by Houk and co-workers by using ω B97XD functional with extended 6-311++G(d) basis set in THF (reaction R1) and acetonitrile (MeCN) (reactions R2 and R3).²⁶ Here we used the same implicit solvation model (SMD) with the aforementioned functionals with 6-31G basis set. Furthermore the final *endo:exo* ratio based on free energy TS barriers of the two forms is with experiments reported on these reactions.²⁷⁻²⁹

We first report in the top panel of Figure 7 the difference of the free energy barriers between *endo* and *exo* approaches, as obtained by present calculations with 6-31G basis set and compared with what was reported by Houk and co-workers. In Table 4 we list all the associated values. We first notice that the basis set has a small effect (as noticed in benchmark calculations), in fact ω B97XD calculations done with the 6-31G basis set are very similar to what reported by Houk and co-workers with the same functional but larger

basis set. Furthermore, also other functionals report values quite close to those ones, where CAM-B3LYP shows a slightly larger difference.

Calculations reported with the extended basis set are done with the methyl group for reaction R3 (R=Me in Scheme 2) while experiments were done with a benzyl group (R=Bn in Scheme 2). We have thus performed calculations with 6-31G basis set with both R=Me and Bn and the corresponding reactions are noted as R3-model and R3-real. Free energy barriers and *endo-exo* differences vary relatively little moving from Me to Bn group, and we will discuss more in details this aspect comparing our results directly with experimental data.

In fact, the experimental *endo:exo* ratios were reported for these reactions. We have calculated them simply from the transition state free energy barriers of *endo* and *exo* forms. Results obtained from experiments and calculations are reported in the bottom panel of Figure 7. We should recall here that, from the experimental results, only the *endo* form is obtained for R3. This experimental finding is translated into an *endo:exo* ratio larger than 20.

Results show that for reactions R1 and R2 the different functionals with 6-31G basis set are in quite good agreement with experiments (and previous calculations). Notably, for reaction R1, where ω B97XD/6-311++G(d) calculations overestimate the *endo* ration, our results are better or equivalent (with a much lower computational cost). Moving to reaction R2, experimentally a slight decrease of *endo:exo* ratio is noticed experimentally, while almost all calculations show the opposite (as well as the previously reported ω B97XD/6-311++G(d) ones), with the exception of M11, which however overestimates this ratio for both reactions. We should notice that the *endo:exo* ratio is very sensitive to small modification in free energy difference, since it has an exponential dependence on $\Delta\Delta G$.

For reaction R3, in the previous work of Ramirez et al. the methyl group was considered and the *endo:exo* ratio was considerably lower than 20 (even lower than the other reactions). We tested for reaction R3 both methyl (called here and hereafter R3-model) and benzyl

group (called here and hereafter R-real), this last being the same as in experiments. Results show that in many cases the *endo:exo* ratio is increased with respect to R3-model. This is particularly evident for LC- ω PBE/D3BJ and MN12SX results which are best in agreement with experiments with an *endo:exo* ratio larger than 20.

Conclusions

The aim of the present work is to find a reliable and affordable electronic structure-based strategy to efficiently describe, real-life, Diels-Alder reactions in the most accurate way possible. We have thus investigated the opportunity of applying reduced-cost electronic structure methods to study such reactions in order to predict reliable characteristic energy barriers. On a series of six reactions, we extensively analysed the performances of a number of recent and traditional DFT functionals (Table 1), with different basis sets, and SEHs, including in many cases empirical dispersion corrections, due to the known deficiencies of such approximated methods in treating long-range electron correlations.⁹⁶ All employed methods are commonly available in general electronic structure codes widely used in the Computational chemistry community.

In a first stage, a specific attention has been put on the role of BSSE when using DFT, testing the quality of reaction barriers predicted using different small-medium size basis sets on two relatively small reactions (reactions B1 and B2 in Scheme 1), for which BSSE effects have been explicitly analyzed by comparing the DFT results to reference CCSD(T)/CBS calculations. In most cases, a good compromise has been found using the 6-31G Pople’s basis set due to a non-negligible error compensation due to the BSSE. In particular, range-separated functionals with dispersion corrections provide good quality results despite the modest basis set size and therefore greatly reduce the computational cost of the simulations. On the other hand, as one could expect, HF and SEHs are shown to be quite ineffective, even with the new SEH parametrizations and dispersion corrections.

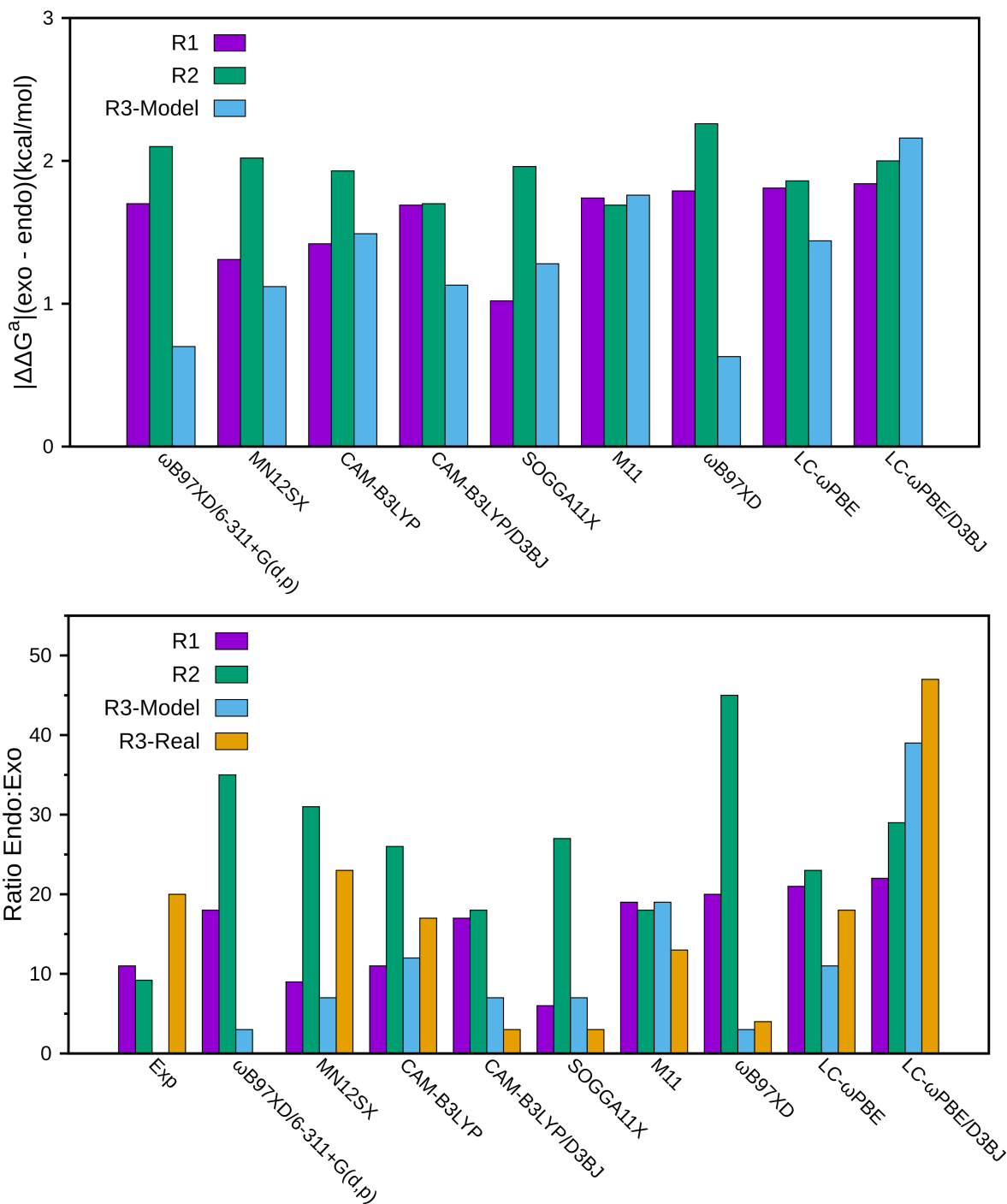


Figure 7: Top) $\Delta\Delta G^\ddagger$ between Exo and Endo TS structures for Cyclic Allene Dienophiles reactions (values are in kcal/mol) for different functionals with 6-31G compared with results from Houk and co-workers obtained at $\omega\text{B97XD}/6\text{-}311\text{+G(d,p)}$ level of theory in implicit solvent. Bottom) Endo:Exo ratio for Cyclic Allene Dienophiles reactions for different functionals with 6-31G basis set, compared with results from Houk and co-workers obtained at $\omega\text{B97XD}/6\text{-}311\text{+G(d,p)}$ level of theory and experiments; reaction R3 is either a simplified model to reduce the number of atoms and so the computational cost (R3-Model), as done by Houk and co-workers ($\omega\text{B97XD}/6\text{-}311\text{+G(d,p)}$), either the real system (R3-Real).

Table 4: ΔG^\ddagger for endo and exo structures, $\Delta\Delta G^\ddagger$ and *endo:exo* ratio for reactions R1, R2 and R3. Energies are in kcal/mol. ω B97XD/6-311++G(d) values are taken from Ramirez et al.,²⁶ which also reports the experimental values for *endo:exo* ratios.

	Endo	Exo	$\Delta\Delta G^\ddagger$	Ratio
R1				
CAM-B3LYP/6-31G	21.81	23.23	1.42	11:1
CAM-B3LYP-GD3BJ/6-31G	17.71	19.39	1.69	17:1
LC- ω PBE/6-31G	22.21	24.02	1.81	21:1
LC- ω PBE-GD3BJ/6-31G	17.46	19.30	1.84	22:1
ω B97XD/6-31G	18.58	20.37	1.79	20:1
SOGGA11X/6-31G	20.32	21.33	1.02	5.5:1
M11/6-31G	18.68	20.42	1.74	19:1
MN12SX/6-31G	17.63	18.94	1.31	9:1
ω B97XD/6-311++G(d)	19.40	21.1	1.7	18:1
Experiments				11:1
R2				
CAM-B3LYP/6-31G	20.86	22.80	1.93	26:1
CAM-B3LYP-GD3BJ/6-31G	15.97	17.67	1.70	18:1
LC- ω PBE/6-31G	21.49	23.35	1.86	23:1
LC- ω PBE-GD3BJ/6-31G	15.45	17.45	2.00	29:1
ω B97XD/6-31G	16.39	18.64	2.26	45:1
SOGGA11X/6-31G	19.11	21.07	1.96	27:1
M11/6-31G	17.10	18.80	1.69	17:1
MN12SX/6-31G	13.00	13.54	0.53	31:1
ω B97XD/6-311++G(d)	17.4	19.5	2.1	35:1
Experiments				9.2:1
R3 (R=Me)				
CAM-B3LYP/6-31G	23.56	25.05	1.49	12:1
CAM-B3LYP-GD3BJ/6-31G	17.41	18.54	1.12	7:1
LC- ω PBE/6-31G	24.34	25.77	1.44	11:1
LC- ω PBE-GD3BJ/6-31G	16.96	19.12	2.16	39:1
ω B97XD/6-31G	17.79	18.42	0.63	3:1
SOGGA11X/6-31G	21.83	22.95	1.13	7:1
M11/6-31G	18.75	20.50	1.76	19:1
MN12SX/6-31G	17.57	18.69	1.12	7:1
ω B97XD/6-311++G(d)	21.0	21.70	0.70	3.3:1
R3 (R=Benzyl)				
CAM-B3LYP/6-31G	24.21	25.84	1.63	16:1
CAM-B3LYP-GD3BJ/6-31G	17.79	18.42	0.64	3:1
LC- ω PBE/6-31G	24.95	26.62	1.67	17:1
LC- ω PBE-GD3BJ/6-31G	16.45	18.73	2.28	47:1
ω B97XD/6-31G	17.89	18.75	0.86	4:1
SOGGA11X/6-31G	22.24	22.86	0.59	3:1
M11/6-31G	18.10	19.60	1.50	13:1
MN12SX/6-31G	17.17	19.04	1.86	23:1
Experiments				> 20:1

We have then applied the best DFT methods to the prediction of three different Diels-Alder reactions in solution using the small 6-31G basis set. We found that they are able to correctly describe the experimentally observed *endo:exo* ratios while free energy barriers appear in agreement with computations performed with an extended basis set.²⁶ Furthermore, the use of such affordable computational approach enables to consider the full complexity of the most extended considered system and therefore to obtain results in better agreement with experiments than those using a slightly reduced model (used in the Literature data). This paves the way for studying either very large systems and/or to use QM/MM dynamics in solutions for Diels-Alder reactions, achieving an high level of accuracy and thus reliable, but cost-effective, predictions.

Concluding, we suggest that the best functionals to be used in future studies on Diels-Alder reactions (in association with the 6-31G basis) should be : ω B97XD, LC- ω PBE/D3BJ, CAM-B3LYP/D3BJ, M11 and MN12SX. It will be surely interesting to understand how (and if) they can be successfully applied also to model other organic reactions.

Supporting Material

In the Supporting Information we report: (i) a pdf file with additional Tables mentioned in the manuscript; (ii) a tar file with xyz structures used in CCSD(T)/CBS calculations of B1, B2 and B3 reactions.

Acknowledgments

RS and DL have a special thank to E.Mentana, A.Sardoni, P.Celata and M.Damilano for their moral support.

References

- (1) Briou, B.; Améduri, B.; Boutevi, B. Trends in the Diels–Alder reaction in polymer chemistry. *Chem. Soc. Rev.* **2021**, *50*, 11055–11097.
- (2) Sara, A. A.; Um-e-Farwa,; Saeed, A.; Kalesse, M. Recent Applications of the Diels–Alder Reaction in the Synthesis of Natural Products (2017–2020). *Synthesis* **2021**, *53*, A–X.
- (3) Pardo, L.; Branchadell, V.; Oliva, A.; Bertran, J. Solvent effect in the Diels–Alder reaction. *J. Mol. Struct. THEOCHEM* **1983**, *10*, 255–260.
- (4) Cativeira, C.; Garcia, J. I.; Mayoral, J. A.; Salvatella, L. Modeling of solvent effects on the Diels–Alder reaction. *Chem. Soc. Rev.* **1996**, *25*, 209–218.
- (5) Zhang, X.; Lefebvre, P. L.; Harvey, J. N. Effect of solvent motions on the dynamics of the Diels–Alder reaction. *Phys. Chem. Chem. Phys.* **2022**, *24*, 1120–1130.
- (6) Loco, D.; Spezia, R.; Cartier, F.; Chataigner, I.; Piquemal, J.-P. Solvation Effects Drive the Selectivity in Diels–Alder Reaction Under Hyperbaric Conditions. *Chem. Comm.* **2020**, *56*, 6632–6634.
- (7) Hu, H.; Kobrak, M. N.; Xu, C.; Hammes-Schiffer, S. Reaction Path Hamiltonian Analysis of Dynamical Solvent Effects for a Claisen Rearrangement and a Diels–Alder Reaction. *J. Phys. Chem. A* **2000**, *104*, 8058–8066.
- (8) Acevedo, O.; Jorgensen, W. L. Understanding Rate Accelerations for Diels–Alder Reactions in Solution Using Enhanced QM/MM Methodology. *J. Chem. Theory Comput.* **2007**, *3*, 1412–1419.
- (9) Black, K.; Liu, P.; Xu, L.; Doubleday, C.; Houk, K. N. Dynamics, transition states, and timing of bond formation in Diels–Alder reactions. *Proc. Natl. Acad. Sci. USA* **2012**, *109*, 12860–12865.

- (10) Yang, Z.; Zou, L.; Yu, Y.; Liu, F.; Dong, X.; Houk, K. N. Molecular dynamics of the two-stage mechanism of cyclopentadiene dimerization: concerted or stepwise? *Chem. Phys.* **2018**, *514*, 120–125.
- (11) Ess, D. H.; Wheeler, S. E.; Iafe, R. G.; Xu, L.; Pelebi-Olcum, N.; Houk, K. N. Bifurcations on Potential Energy Surfaces of Organic Reactions. *Org. Lett.* **2018**, *20*, 2821–2825.
- (12) Hare, S. R.; Li, A.; Tantillo, D. J. Post-transition state bifurcations induce dynamical detours in Pummerer-like reactions. *Chem. Sci.* **2018**, *9*, 8937–8945.
- (13) Carpenter, B. K.; Harvey, J. N.; Glowacki, D. R. Prediction of enhanced solvent-induced enantioselectivity for a ring opening with a bifurcating reaction path. *Phys. Chem. Chem. Phys.* **2015**, *17*, 8372–8381.
- (14) Tan, J. S. J.; Hirvonen, V.; Paton, R. S. Dynamic Intermediates in the Radical Cation Diels-Alder Cycloaddition: Lifetime and Suprafacial Stereoselectivity. *Org. Lett.* **2018**, *20*, 2821–2825.
- (15) Kelly, K. K.; Hirschi, J. S.; Singleton, D. A. Newtonian Kinetic Isotope Effects. Observation, Prediction, and Origin of Heavy-Atom Dynamic Isotope Effects. *J. Am. Chem. Soc.* **2009**, *131*, 8382–8383.
- (16) Mardirossian, N.; Head-Gordon, M. Characterizing and Understanding the Remarkably Slow Basis Set Convergence of Several Minnesota Density Functionals for Intermolecular Interaction Energies. *J. Chem. Theory Comput.* **2013**, *9*, 4453–4461.
- (17) Pieniazek, S. N.; Clemente, F. R.; Houk, K. N. Sources of Error in DFT Computations of C–C Bond Formation Thermochemistries: $\pi \rightarrow \sigma$ Transformations and Error Cancellation by DFT Methods. *Angew. Chem. Int. Ed.* **2008**, *47*, 7746–7749.

- (18) Kruse, H.; Goerigk, L.; Grimme, S. Why the Standard B3LYP/6-31G* Model Chemistry Should Not Be Used in DFT Calculations of Molecular Thermochemistry: Understanding and Correcting the Problem. *J. Org. Chem.* **2012**, *77*, 10824–10834.
- (19) Li, H.; Tirri, B.; Brémond, E.; Sancho-García, J. C.; Adamo, C. Beyond Chemical Accuracy for Alkane Thermochemistry: The DHthermo Approach. *J. Org. Chem.* **2021**, *86*, 5538–5545.
- (20) Martin-Somer, A.; Macaluso, V.; Barnes, G. L.; Yang, L.; Pratihar, S.; Song, K.; Hase, W. L.; Spezia, R. Role of Chemical Dynamics Simulations in Mass Spectrometry Studies of Collision-Induced Dissociation and Collisions of Biological Ions with Organic Surfaces. *J. Am. Soc. Mass Spectrom.* **2020**, *31*, 2–24.
- (21) Carrá, A.; Spezia, R. In silico tandem mass spectrometer: an analytical and fundamental tool. *Chemistry – Methods* **2021**, *1*, 123–130.
- (22) Nieman, R.; Spezia, R.; Jayee, B.; Minton, T.; Hase, W. L.; Guo, H. Exploring Reactivity and Product Formation in N(4S) Collisions with Pristine and Defected Graphene with Direct Dynamics Simulations. *J. Chem. Phys.* **2020**, *153*, 184702.
- (23) Malik, A.; Spezia, R.; Hase, W. L. Unimolecular Fragmentation Properties of Thermometer Ions from Chemical Dynamics Simulations. *J. Am. Soc. Mass Spectrom.* **2021**, *32*, 169–179.
- (24) Meuwly, M. Machine Learning for Chemical Reactions. *Chem. Rev.* **2021**, *121*, 10218–10239.
- (25) Lewis-Atwell, T.; Townsend, P. A.; Grayson, M. N. Machine learning activation energies of chemical reactions. *WIREs Comput. Mol. Sci.* **2021**, e1593.
- (26) Ramirez, M.; Svatunek, D.; Liu, F.; Garg, N. K.; Houk, K. N. Origins of Endo Selectivity

- in Diels–Alder Reactions of Cyclic Allene Dienophiles. *Angew. Chem. Int. Ed.* **2021**, *60*, 14989–14997.
- (27) Lofstrand, V. A.; West, F. G. Efficient Trapping of 1,2-Cyclohexadienes with 1,3-Dipoles. *Chem. Eur. J.* **2016**, *22*, 10763–10767.
- (28) Yamano, M. M.; Knapp, R. R.; Ngamnithiporn, A.; Ramirez, M.; Houk, K. N.; Stoltz, B. M.; Garg, N. K. Cycloadditions of Oxacyclic Allenes and a Catalytic Asymmetric Entryway to Enantioenriched Cyclic Allenes. *Angew. Chem. Int. Ed.* **2019**, *58*, 5653–5657.
- (29) Barber, J. S.; Yamano, M. M.; Ramirez, M.; Darzi, E. R.; Knapp, R. R.; Liu, F.; Houk, K. N.; Garg, N. K. Diels–Alder cycloadditions of strained azacyclic allenenes. *Nature Chem.* **2018**, *10*, 953–960.
- (30) Chataigner, I.; Hess, E.; Toupet, L.; Piettre, S. R. Activation of the Dienophilicity of Indoles in Normal Electron Demand [4 + 2] Cycloadditions under High Pressure. *Org. Lett.* **2001**, *3*, 515–519.
- (31) Chrétien, A.; Chataigner, I.; L'Hélias, N.; S. R. Piettre, S. R. Complete and remarkable reversal of chemoselectivity in [4 + 2] cycloadditions involving electron-poor indoles as dienophiles. Diels-Alder versus hetero-Diels-Alder processes. *J. Org. Chem.* **2003**, *6*, 7990–8002.
- (32) Teyssot, M.-L.; Lormier, A.-T.; Chataigner, I.; Piettre, S. Cross-Diels-Alder reactions of 6-oxo-1-sulfonyl-1,6-dihydropyridine-3-carboxylates. *J. Org. Chem.* **2007**, *72*, 2364–2373.
- (33) Chopin, N.; Gérard, H.; Chataigner, I.; Piettre, S. Benzofurans as Efficient Dienophiles in Normal Electron Demand [4 + 2] Cycloadditions. *J. Org. Chem.* **2009**, *74*, 1237–1246.

- (34) Rkein, B.; Bigot, A.; Birbaum, L.; Manneveau, M.; Paolis, M. D.; Legros, J.; Chataigner, I. Reactivity of 3-nitroindoles with electron-rich species. *Chem. Comm.* **2021**, *57*, 27–44.
- (35) Rkein, B.; Manneveau, M.; Noël-Duchesneau, L.; Pasturaud, K.; Durandetti, M.; Legros, J.; Lakhdar, S.; Chataigner, I. How electrophilic are 3-nitroindoles? Mechanistic investigations and application to a reagentless (4+2) cycloaddition. *Chem. Comm.* **2021**, *57*, 10071–10074.
- (36) Woodward, R. B.; Baer, H. The Reaction of Furan with Maleic Anhydride. *J. Am. Chem. Soc.* **1948**, *70*, 1161–1166.
- (37) Eggelte, T. A.; Koning, H. D.; Huisman, H. O. Synthesis and some reductions of endo- and exo-3,6-epoxy- Δ^4 -tetrahydrophthalic anhydride. *Tetrahedron* **1973**, *29*, 2445–2447.
- (38) Rulisek, L.; Sebek, P.; Havlas, Z.; Hrabal, R.; Capek, P.; Svatos, A. An Experimental and Theoretical Study of Stereoselectivity of Furan-Maleic Anhydride and Furan-Maleimide Diels-Alder Reactions. *J. Org. Chem.* **2005**, *70*, 6295–6302.
- (39) Drinkuth, S.; Groetsch, S.; Peters, E.-M.; Peters, K.; Christl, M. 1-Methyl-1-azacyclohexa-2,3-diene(N-B)borane - Generation and Interception of an Unsymmetrical Isodihydropyridine. *Eur. J. Org. Chem.* **2001**, *2001*, 2665–2670.
- (40) Elliott, R. L.; Nicholson, N. H.; Peaker, F. E.; Takle, A. K.; Tyler, J. W.; White, J. Cycloadditions of cephalosporins. The formation of [4+2] adducts with 5-membered heterocycles. *J. Org. Chem.* **1994**, *59*, 1606–1607.
- (41) Frisch, M. J. et al. Gaussian~16 Revision C.01. 2016; Gaussian Inc. Wallingford CT.
- (42) Stewart, J. J. P. MOPAC2016, Version: 18.011L. 2016; Stewart Computational Chemistry, web-site: [HTTP://OpenMOPAC.net](http://OpenMOPAC.net).

- (43) Helgaker, T.; Klopper, W.; Koch, H.; Noga, J. Basis-set convergence of correlated calculations on water. *J. Chem. Phys.* **1997**, *106*, 9639–9646.
- (44) Řezáč, J.; Hobza, P. Describing Noncovalent Interactions beyond the Common Approximations: How Accurate Is the “Gold Standard,” CCSD(T) at the Complete Basis Set Limit? *J. Chem. Theory Comput.* **2013**, *9*, 2151–2155.
- (45) Grimme, S.; Ehrlich, S.; Goerigk, L. Effect of the damping function in dispersion corrected density functional theory. *J. Comp. Chem.* **2011**, *32*, 1456–1465.
- (46) Grimme, S. Semiempirical GGA-type density functional constructed with a long-range dispersion correction. *J. Comp. Chem.* **2006**, *27*, 1787–1799.
- (47) Grimme, S.; Antony, J.; Ehrlich, S.; Krieg, H. A consistent and accurate ab initio parameterization of density functional dispersion correction (DFT-D) for the 94 elements H-Pu. *J. Chem. Phys.* **2010**, *132*, 154104.
- (48) Hohenberg, P.; Kohn, W. Inhomogeneous Electron Gas. *Phys. Rev.* **1964**, *136*, B864–B871.
- (49) Kohn, W.; Sham, L. J. Self-Consistent Equations Including Exchange and Correlation Effects. *Phys. Rev.* **1965**, *140*, A1133–A1138.
- (50) S. H. Vosko, L. W.; Nusair, M. Accurate spin-dependent electron liquid correlation energies for local spin density calculations: A critical analysis. *Can. J. Phys.* **1980**, *58*, 1200–1211.
- (51) Becke, A. D. Density-functional exchange-energy approximation with correct asymptotic-behavior. *Phys. Rev. A* **1988**, *38*, 3098–3100.
- (52) Lee, C.; Yang, W.; Parr, R. G. Development of the Colle-Salvetti correlation-energy formula into a functional of the electron density. *Phys. Rev. B* **1988**, *37*, 785–789.

- (53) Miehlich, B.; Savin, A.; Stoll, H.; Preuss, H. Results obtained with the correlation-energy density functionals of Becke and Lee, Yang and Parr. *Chem. Phys. Lett.* **1989**, *157*, 200–206.
- (54) Perdew, J. P.; Burke, K.; Ernzerhof, M. Generalized gradient approximation made simple. *Phys. Rev. Lett.* **1996**, *77*, 3865.
- (55) Hamprecht, F. A.; Cohen, A.; Tozer, D. J.; Handy, N. C. Development and assessment of new exchange-correlation functionals. *J. Chem. Phys.* **1998**, *109*, 6264–6271.
- (56) Grimme, S. Semiempirical GGA-type density functional constructed with a long-range dispersion correction. *J. Comp. Chem.* **2006**, *27*, 1787–1799.
- (57) Grimme, S.; Ehrlich, S.; Goerigk, L. Effect of the damping function in dispersion corrected density functional theory. *J. Comp. Chem.* **2011**, *32*, 1456–1465.
- (58) Gill, P. M. W. A new gradient-corrected exchange functional. *Mol. Phys.* **1996**, *89*, 433–445.
- (59) Perdew, J. P. Density-functional approximation for the correlation energy of the inhomogeneous electron gas. *Phys. Rev. B* **1986**, *33*, 8822–8824.
- (60) Peverati, R.; Zhao, Y.; Truhlar, D. G. Generalized Gradient Approximation That Recovers the Second-Order Density-Gradient Expansion with Optimized Across-the-Board Performance. *J. Phys. Chem. Lett.* **2011**, *2*, 1991–1997.
- (61) Becke, A. D. Density-functional thermochemistry. III. The role of exact exchange. *J. Chem. Phys.* **1993**, *98*, 5648–5652.
- (62) Adamo, C.; Barone, V. Toward reliable density functional methods without adjustable parameters: The PBE0 model. *J. Chem. Phys.* **2011**, *110*, 6158–6169.

- (63) Perdew, J. P.; Burke, K.; Wang, Y. Generalized gradient approximation for the exchange-correlation hole of a many-electron system. *Phys. Rev. B* **1996**, *54*, 16533–16539.
- (64) Becke, A. D. Density-functional thermochemistry. IV. A new dynamical correlation functional and implications for exact-exchange mixing. *J. Chem. Phys.* **1996**, *104*, 1040–1046.
- (65) Adamo, C.; Barone, V. Exchange functionals with improved long-range behavior and adiabatic connection methods without adjustable parameters: The mPW and mPW1PW models. *J. Chem. Phys.* **1998**, *108*, 664–675.
- (66) Austin, A.; Petersson, G.; Frisch, M. J.; Dobek, F. J.; Scalmani, G.; Throssell, K. A density functional with spherical atom dispersion terms. *J. Chem. Theory Comput.* **2012**, *8*, 4989.
- (67) Peverati, R.; Truhlar, D. G. A global hybrid generalized gradient approximation to the exchange-correlation functional that satisfies the second-order density-gradient constraint and has broad applicability in chemistry. *J. Chem. Phys.* **2011**, *135*, 191102.
- (68) Tao, J. M.; Perdew, J. P.; Staroverov, V. N.; Scuseria, G. E. Climbing the density functional ladder: Nonempirical meta-generalized gradient approximation designed for molecules and solids. *Phys. Rev. Lett.* **2003**, *91*, 146401.
- (69) Van Voorhis, T.; Scuseria, G. E. A novel form for the exchange-correlation energy functional. *J. Chem. Phys.* **1998**, *109*, 400–410.
- (70) Boese, A. D.; Handy, N. C. New exchange-correlation density functionals: The role of the kinetic-energy density. *J. Chem. Phys.* **2002**, *116*, 9559–9569.
- (71) Zhao, Y.; Truhlar, D. G. A new local density functional for main-group thermochem-

- istry, transition metal bonding, thermochemical kinetics, and noncovalent interactions. *J. Chem. Phys.* **2006**, *125*, 1–18.
- (72) Zhao, Y.; Truhlar, D. G. The M06 suite of density functionals for main group thermochemistry, thermochemical kinetics, noncovalent interactions, excited states, and transition elements: two new functionals and systematic testing of four M06-class functionals and 12 other functionals. *Theor. Chem. Acc.* **2008**, *120*, 215–241.
- (73) Zhao, Y.; Truhlar, D. G. Density Functional for Spectroscopy: No Long-Range Self-Interaction Error, Good Performance for Rydberg and Charge-Transfer States, and Better Performance on Average than B3LYP for Ground States. *J. Phys. Chem. A* **2006**, *110*, 13126–13130.
- (74) Boese, A. D.; Martin, J. M. L. Development of Density Functionals for Thermochemical Kinetics. *J. Chem. Phys.* **2004**, *121*, 3405–3416.
- (75) Yanai, T.; Tew, D.; Handy, N. A new hybrid exchange-correlation functional using the Coulomb-attenuating method (CAM-B3LYP). *Chem. Phys. Lett.* **2004**, *393*, 51–57.
- (76) Chai, J.-D.; Head-Gordon, M. Long-range corrected hybrid density functionals with damped atom-atom dispersion corrections. *Phys. Chem. Chem. Phys.* **2008**, *10*, 6615–6620.
- (77) Chai, J.-D.; Head-Gordon, M. Systematic optimization of long-range corrected hybrid density functionals. *J. Chem. Phys.* **2008**, *128*, 084106.
- (78) Heyd, J.; Scuseria, G. Efficient hybrid density functional calculations in solids: The HS-Ernzerhof screened Coulomb hybrid functional. *J. Chem. Phys.* **2004**, *121*, 1187–1192.
- (79) T. M. Henderson, G. E. S., A. F. Izmaylov; Savin, A. Assessment of a middle range hybrid functional. *J. Chem. Theory Comput.* **2008**, *4*, 1254.

- (80) Vydrov, O. A.; Scuseria, G. E. Assessment of a long range corrected hybrid functional. *J. Chem. Phys.* **2006**, *125*, 234109.
- (81) Peverati, R.; Truhlar, D. G. Screened-exchange density functionals with broad accuracy for chemistry and solid state physics. *Phys. Chem. Chem. Phys.* **2012**, *14*, 16187.
- (82) Peverati, R.; Truhlar, D. G. Improving the Accuracy of Hybrid Meta-GGA Density Functionals by Range Separation. *J. Phys. Chem. Lett.* **2011**, *2*, 2810–2817.
- (83) Peverati, R.; Truhlar, D. G. Exchange-Correlation Functional with Good Accuracy for Both Structural and Energetic Properties while Depending Only on the Density and Its Gradient. *J. Chem. Theory Comput.* **2012**, *8*, 2310–2319.
- (84) Peverati, R.; Truhlar, D. G. M11-L: A Local Density Functional That Provides Improved Accuracy for Electronic Structure Calculations in Chemistry and Physics. *J. Phys. Chem. Lett.* **2012**, *3*, 117–124.
- (85) Peverati, R.; Truhlar, D. G. An improved and broadly accurate local approximation to the exchange–correlation density functional: The MN12-L functional for electronic structure calculations in chemistry and physics. *Phys. Chem. Chem. Phys.* **2012**, *10*, 13171.
- (86) Grimme, S. Semiempirical hybrid density functional with perturbative second-order correlation. *J. Chem. Phys.* **2006**, *124*, 034108.
- (87) Boys, S. F.; Bernardi, F. Calculation of Small Molecular Interactions by Differences of Separate Total Energies – Some Procedures with Reduced Errors. *Mol. Phys.* **1970**, *19*, 553.
- (88) Marenich, A. V.; Cramer, C. J.; Truhlar, D. G. Universal solvation model based on solute electron density and a continuum model of the solvent defined by the bulk dielectric constant and atomic surface tensions. *J. Phys. Chem. B* **2009**, *113*, 6378–6396.

- (89) Dewar, M. J. S.; Zoebisch, E. G.; Healy, E. F.; Stewart, J. J. P. Development and use of quantum mechanical molecular models. 76. AM1: A new general purpose quantum mechanical molecular model. *J. Am. Chem. Soc.* **1985**, *107*, 3902.
- (90) Rocha, G. B.; Freire, R. O.; Simas, A. M.; Stewart, J. J. P. RM1: A Reparameterization of AM1 for H, C, N, O, P, S, F, Cl, Br, and I. *J. Comp. Chem.* **2006**, *27*, 1101–1111.
- (91) Stewart, J. J. P. Optimization of parameters for semiempirical methods I. Method. *J. Comput. Chem.* **1989**, *10*, 209–220.
- (92) Stewart, J. J. P. Optimization of parameters for semiempirical methods. V. Modification of NDDO approximations and application to 70 elements. *J. Mol. Model.* **2007**, *13*, 1173–1213.
- (93) Rezac, J.; Hobza, P. Advanced Corrections of Hydrogen Bonding and Dispersion for Semiempirical Quantum Mechanical Methods. *J. Chem. Theory Comput.* **2012**, *8*, 141–151.
- (94) Stewart, J. J. P. Optimization of parameters for semiempirical methods VI: more modifications to the NDDO approximations and re-optimization of parameters. *J. Mol. Model.* **2013**, *19*, 1–32.
- (95) Grimme, S. Accurate description of van der Waals complexes by density functional theory including empirical corrections. *J. Comp. Chem.* **2004**, *25*, 1463–1473.
- (96) Grimme, S.; Hansen, A.; Brandenburg, J. G.; Bannwarth, C. Dispersion-Corrected Mean-Field Electronic Structure Methods. *Chem. Rev.* **2016**, *116*, 5105–5154.
- (97) Wang, Y.; Jin, X.; Yu, H. S.; Truhlar, D. G.; He, X. Revised M06-L functional for improved accuracy on chemical reaction barrier heights, noncovalent interactions, and solid-state physics. *Proc. Nat. Ac. Sci.* **2017**, *114*, 8487–8492.

Graphical TOC Entry

